MEDUSA – Mechanism for Entrapment of Debris Using Shape memory Alloy

Louis Wei-Yu Feng[(1)], Peter Martinez[(1)], Michael Dropmann[(2)], Manfred Ehresmann[(2)], Samuel Ginsberg[(1)], Georg Herdrich[(2)], Rene Laufer[(1),(3)]

(1) SpaceLab, Department of Electrical Engineering, University of Cape Town, Rondebosch, South Africa
Email: wei.yu.louis.feng@gmail.com, peter.martinez@uct.ac.za, samuel.ginsberg@uct.ac.za, rene.laufer@uct.ac.za
(2) Institute for space systems (IRS), University of Stuttgart, Pfaffenwaldring 29, 70569 Stuttgart, Germany
Email: herdrich@irs.uni-stuttgart.de, ehresmann@irs.uni-stuttgart.de, dropmann@irs.uni-stuttgart.de
(3) Center for Astrophysics, Space Physics and Engineering Research (CASPER), Baylor University, One Bear Place #97310, Waco, TX, USA
Email: rene_laufer@baylor.edu

ABSTRACT

Active space debris removal is becoming an important area of research due to the rapid growth of space debris and the need for some form of debris remediation. Debris remediation concepts fall into two general categories: contact-based and contactless. Contact-based schemes for debris capture have to overcome the challenge of capturing a non-cooperating object in space with no pre-designed attachment points. Various schemes involving, inter alia, nets and harpoons have been proposed. In this paper we explore the potential to use shape-memory alloys as a technological basis for a debris capturing solution that can be used multiple times. A proof-of-concept prototype was developed at the University of Cape Town, named MEDUSA (Mechanism for Entrapment of Debris Using Shape memory Alloy). This has been designed as a validation payload for a CubeSat test platform to perform a small debris capture proof-of-concept demonstration. MEDUSA uses the shape-memory alloy nitinol, which gives it the ability to assume pre-programmed "open" and "closed" shapes after distortion. Each of the five arms of MEDUSA can attain both pre-programmed shapes to allow reversible operations. This paper presents the design and development process from the conceptual design to the current Mk-III prototype which is built on improvements made from the Mk-II prototype discussed in an earlier publication [1]. The device has undergone vacuum and partial thermal testing at the Institute for Space Systems (IRS) in Stuttgart to assess its performance under various environmental conditions.

1 INTRODUCTION

CubeSats have become a popular platform for various space missions due to their low cost, short development time and flexible launching options. Many academic researchers have embraced CubeSats as an alternative to traditional satellites that are much more expensive.

More than one hundred CubeSats were placed in LEO up to end of 2012 and a further 80 CubeSats were launched by the end of 2013 [2].

However, CubeSats typically have a very limited operational lifetime and very minimum capabilities for propulsion. Once they are no longer functional, CubeSats join the growing population of space debris in LEO that poses risks on LEO satellites. Factors such as lack of de-orbiting technologies and absence of regulations that promote passive de-orbiting also leads to CubeSats being associated with the debris.

During a collision between debris and an active spacecraft an energy ratio of 1:1250 [3] is released. For instance, debris with 240 grams will catastrophically destroy a 300 kilogram satellite due to the high kinetic energy from its orbital speed. To date, there have been at least four reported debris-on-satellite collision incidents.

With each collision, the number of orbital fragments multiplies, which if unchecked could result in a cascading effect of debris multiplication referred to as the Kessler syndrome. At current launch rates, the increase of space objects in LEO is outpacing their removal by natural processes. Thus remediation measures are needed. The concept of active debris removal (ADR) was proposed approximately 25 years ago. Several approaches of ADR have been explored by a variety of authors. These fall in to two main categories: contact and non-contact. Non-contacting methods include the use of lasers to change debris orbits by ablation. The contact based methods of ADR involve actively capturing the target and then performing a re-entry. The orbital region to apply ADR missions to make it most effective is in LEO that has been addressed in sveral sources [3-5].

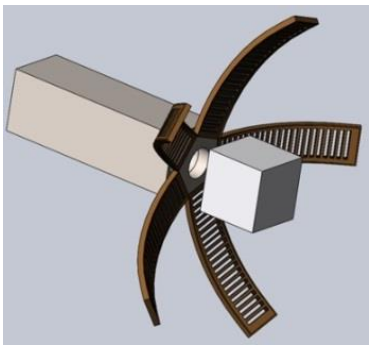

Figure. 1: Mechanism for Entrapment of Debris Using Shape memory Alloy (MEDUSA). Conceptual Design shown implemented on a 3-U CubeSat chaser spacecraft.

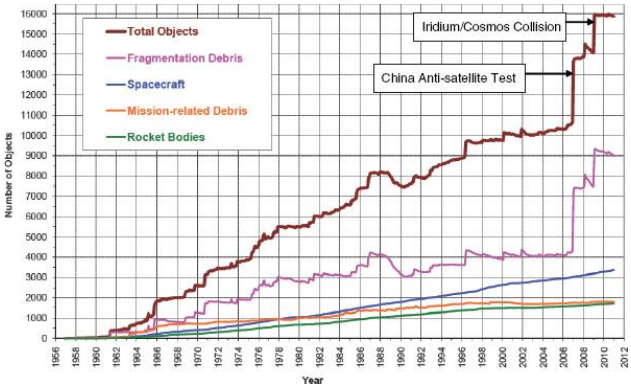

Figure. 2: Number of tracked objects in LEO and their respective sources. [6].

2 CHALLENGES IN ADR

To maintain a constant debris population to prevent the Kessler syndrome, five large targets should be removed annually from LEO starting 2020 [7]. Up to date, docking with an uncooperative object has never been achieved without involving human astronauts [8]. The challenges in target capturing are that the chaser spacecraft must be very flexible and adaptable to different targets and may require pre-knowledge of target shape, size, configuration, tumbling rate and spin axis. Hence, it is important to have a solution that does not rely on specific characteristics or interfaces to the target object.

Debris capturing technologies may be grouped into two main categories: contact-based and contactless. Each of these two approaches has its own advantage and disadvantages. The contact-based methodologies face challenges in the rendezvous phase and during the capturing phase. Contactless technologies tend to have lower requirements on GNC since less complex propulsion systems are needed. However many of the contactless technologies cannot manage a controlled trajectory during de-orbiting. In this paper, we will discuss a capture method that does not require any predefined attachment points on the target object.

The major challenge during the capturing phase is where a large target has both a tumbling motion and numerous structures protruding from the target. Such structures could potentially touch the capturing mechanism during the capturing process and push the target away. Hence without pre-knowledge of the target, the chaser spacecraft becomes heavily dependent on image processing to recognize target configuration shape.

Challenges faced in manoeuvres are that the target has to be flown around, approached and then connected to. This requires the design of a sophisticated system to achieve complex rotational and translational movement in a short response time from the chaser spacecraft. This requires a higher capability of propulsion and Guidance Navigation and Control (GNC) than what is usually installed in spacecraft operating in LEO [8].

3 DESIGN CONCEPT OF MEDUSA

A shape memory alloy (SMA) driven debris capturing mechanism is proposed and developed to lay a proof-of-concept using a CubeSat to perform small-scale ADR missions. This capturing mechanism provides two functional modes, capture and release, to allow multiple attempts of target capturing, unlike some other capturing mechanisms for ADR missions which only allow a single attempt (e.g. net-catching mechanisms and harpoons).

The MEDUSA concept envisages a chaser spacecraft approaching a target object. Once the target object is within the capture volume of the device, a series of arms encircle the target to trap it inside the capturing volume.

The capturing volume is spherical with a volume equivalent to a 5-U CubeSat (5003 cm³), the gaps between the arms must be less than 8 cm to prevent escape of a 1-U sized target. The closing time shall be less than 10 seconds for a swift capture action. Parameters of the spherical capturing volume are tabulated in Tab 1.

Table 1. Parameters of the spherical capturing volume.

Parameter	**Value**
Diameter	21.22 cm
Surface Area	1414.6 cm^2
Volume	5000 cm^3

4 MATERIAL SELECTION

Nitinol consists of 45% nickel and 55% titanium. Nitinol is a shape memory alloy (SMA) that was selected to be the back bone of the capturing arm that further provides the actuating force of the mechanism.

The force is generated during the state transition between the Martensite state and the Austenite state that is used to perform capture and release actions in the MEDUSA application. This allows one to exploit the ability of Nitinol to generate a large force from very small element dimensions and weight. Nitinol's ability of shape recovery and the high generated force during the recovery process make it an excellent candidate. Two sets of nitinol wires were programmed to provide the two functionalities required. One set is programmed with a "C" shape for enclosure and the other with an "L" shape for release. When one shape is being activated the non-active wire will follow the movement of the active wire, due to its softer material properties in the martensite state. Material properties of the used nitinol are tabulated in Tab. 2 [9].

Table 2. Properties of Nitinol.

Characteristics	Values
Density	6.45 gm / cm^2
Thermal Conductivity	10 W / mK
Specific Heat	322 J / kgK
Latent Heat	24 200 J / kg
Ultimate Tensile Strength	750 – 960 MPa
Elongation to Failure	15.5 %
Yield Strength (Austenite)	560 MPa
Young's Modulus (Austenite)	75 GPa
Yield Strength (Martensite)	100 MPa
Young's Modulus (Martensite)	28 GPa

The material selected as the structure to integrate the L- and C-shaped nitinol wires into a single capturing arm is polyamide. The material selection was based on the ability to cope with the harsh space environment as well as to withstand heat dissipation from the nitinol during capture and release operations.

Polyamide is widely used in aerospace industry for its robust thermal properties and its ability to damp vibrations, which may occur when connecting to a tumbling target. Polyamide also is an electric insulator preventing short circuits between separate nitinol wires. The high melting temperature of 260°C and long term service temperature between -40°C to 110°C sufficiently covers the temperature range for CubeSat missions in LEO when respective thermal insulation methods are used as described below. Lastly, polyamide can easily be manufactured using laser cutting to create the patterns required to hold the actuating nitinol wires.

For protection from the space environment a Kapton HN polyimide film is tailored into sheaths used to cover the capturing arms. An example of Kapton HN application is the sun shield on James Webb telescope spacecraft. For thermal insulating purposes a reflective metallic film has to be applied to this cover.

All parts mentioned above integrated form a single capturing arm of MEDUSA as shown in Fig 3.

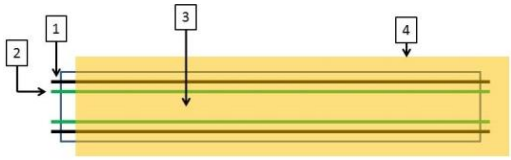

Figure. 3: Conceptual design of a single MEDUSA arm. 1- "C" shaped nitinol, 2- "L" shaped nitinol, 3- "body" made out of polyamide and 4- "sheaths" made out of polyimide.

5 MANUFACTURING

In this section the manufacturing process to complete a single capturing arm is described. The entire manufacturing process is done five times to create five capturing arms as needed for the MEDUSA application. The shape memory programming performed on nitinol is shown in Section 5.1, the laser cutting process for polyamide is shown in Section 5.2 and the protective sheaths manufacturing process is shown in Section 5.3. Lastly the process to integrate all components manufactured is shown in Section 5.4.

5.1 Nitinol selection and programming

The dimensions of the nitinol wires were selected based on two main requirements: electrical power needed to reach the required temperature and the force generated during the transition from the martensite state to the austenite state. Since electrical resistance is inversely proportional to the cross-sectional area, nitinol with a large diameter was preferred. Further, nitinol wires with larger diameter generate a stronger recovery force. After several experiments in the laboratory it was proven that a nitinol wire with 1 mm diameter releases sufficient force to enclose the capturing volume, which was tested in a laboratory environment with one g.

For shape programming two moulds with "C" and "L" shaped grooves were made out of mild steel. The nitinol wires were placed into the grooves of the moulds and then sealed with Kapton tape to hold them firmly in place during shape programming. Then the mould was covered with another mild steel plate and screwed together for a tight fit. During the nitinol programming, an oxidization layer formed due to the high temperatures. This layer had to be removed to ensure good electrical contact between the nitinol wires and the electrical wires.

5.2 Polyamide arms

In order to reduce the resistance of the polyamide

structure to the bending forces generated by the nitinol wires and also to reduce the mass of the arms, a series of cut-out slots were placed along the length of the arm. A pattern was designed to create channels holding the nitinol wires while allowing free movement during actuation. After laser cutting 43% of the original polyamide mass in a 6 cm by 37 cm rectangular strips was extracted. The resultant polyamide strips are much lighter more flexible and agile after excess material was removed and consequently less force is required for actuation.

5.3 Protective sheaths

Kapton HN is well known for its high melting point and electrical insulation ability. Furthermore, Kapton HN is difficult to penetrate, it protects the capturing arms from possible damage of sharp corners or edges from target debris. The thermal insulating property will be added to the protection sheaths equipped onto the final product with a reflective metallic coating. For initial testing bare Kapton HN was used for reasons of simplicity and availability. Once the light reflective material is applied to the Kapton HN surface the radiative heat transfer in space is restricted, helping to keep temperatures at moderate levels.

Kapton HN of 25μm thickness was used to manufacture the protective sheaths that envelope the arms. The Kapton HN sheet was tailored into strips of 40 by 14 cm in dimension, folds over and sealed with Kapton tape.

5.4 Electrical circuit design

The circuit design considers a several contingencies that could lead to a failure of the target capturing mission. One contingency is when the five capturing arms do not deploy simultaneously which introduces a torque onto the chase spacecraft. An additional resultant torque will be caused by unbalanced forces during deployment and act on the chaser spacecraft and disturb its stable attitude state. Thus, the design must have a control system based on hardware capabilities that acts on all capturing arms concurrently. This is achieved by using parallel circuits that supply power to all capturing arms simultaneously.

The control system of MEDUSA consists of two series branches connected in parallel that operate two functions: capture and release. The “C-circuit” denotes the circuit executing the capture function and “R-circuit” denotes the circuit executing the release function. Each of the five capturing arms has 4 loops of nitinol wires installed, 2 C-shaped wires and 2 L-shaped wires, leading to a total of 20 nitinol loops used in MEDUSA. The C-circuit contains 10 nitinol loops. It is further subdivided in two distinct circuits with 5 loops in series, which are then installed in parallel. The same design is applied to the R-circuit. The circuit design is shown schematically in Fig. 4.

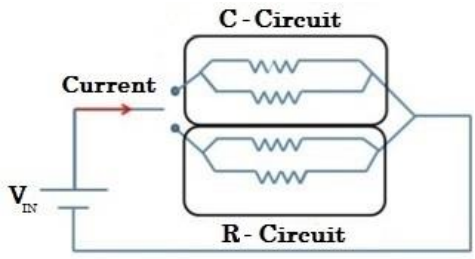

Figure. 4: Control circuit of MEDUSA. Each resistor represents five nitinol loops wired in series, each with 3.48Ω in resistance. Total resistance for the C-circuit and R-circuit are 1.74 Ω each.

5.5 MEDUSA Mk-III Integration

The previously discussed components integrate to form a single capturing arm. Connections between electrical wires and nitinol wires were formed by mechanical clamps rather than soldering because nitinol is difficult to solder. Before electrical connections were established the oxidization layer formed during programming acts as an insulator had to be completely removed.

The completed product of MEDUSA Mk-III without protective cover sheaths is shown in Fig. 5. Each capturing arm weighs 26 grams, while the five protection sheaths weigh 9 grams in total. The arm-mounting plate made of PLA weighs 11 grams and the base, also made out of PLA, used to connect the MEDUSA system and the chaser spacecraft weighs 25 grams. In total the MEDUSA Mk-III weighs 175 grams which is approximately 15% of the allowable mass for a 1-U CubeSat.

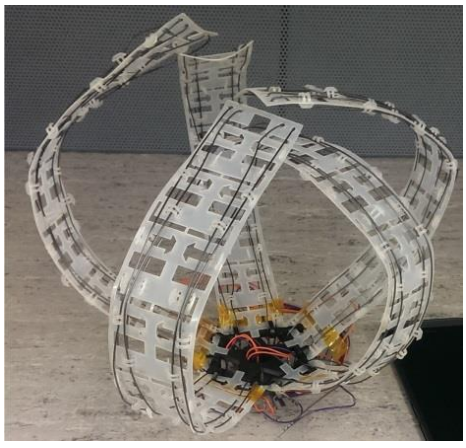

Figure. 5: The completed MEDUSA Mk-III in capturing mode. To enhance the visibility of the structure, the protective Kapton sheaths are not shown.

6 VACUUM CHAMBER TESTS

In order to investigate the operations of MEDUSA under vacuum conditions, a series of tests were

performed in the vacuum chamber PWK1 [11] shown in Fig. 6 that is situated at the IRS. To place MEDUSA inside the vacuum chamber a structure was built using a set of Bosch modular strut profiles as shown in Fig 7.

Figure. 6: Vacuum Chamber PWK1 at IRS, in Stuttgart University.

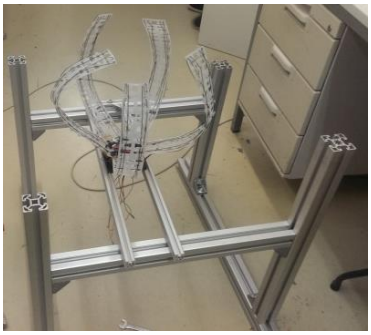

Figure. 7: Supporting frame constructed from Bosch strut profiles. The frame was used to adjust the height of MEDUSA to be visible through the observation windows of PWK1.

Experiments were carried out in both vacuum and for comparison in atmospheric environment. The same capturing arm (arm-2) was used throughout all tests. The experiment was designed to investigate the thermal behaviour of MEDUSA before, during, and after capture and release operations in vacuum and atmospheric conditions. The temperature of MEDUSA arm-2 was recorded at 0.1 seconds intervals while the nitinol wire were being actuated and therefore heating up, and also in the cooling down phase after actuation. A baseline reference temperature of 25℃ was chosen as the starting/ending temperature for actuation (heating) or cooling phases, respectively.

For this thermocouples were installed on the wires and further current and voltage were measured. The test procedure was as follows.

1. The test begins when the thermocouple K1 attached to the C-circuit reads 25 ℃. If nitinol wires were below 25 ℃ an impulse of current was supplied to heat up the nitinol wire to approximately 30 ℃, then it was waited until the temperature dropped to 25 ℃ to start the experiment.
2. Supply 10 V with corresponding current of 5 A into C-circuit in arm-2 until the thermocouple K1 reads 50 ℃.
3. Switch off input voltage.
4. Wait for K1 to drop to 25 ℃.
5. Supply 10 V and 5 A into R-circuit in capturing arm.
6. Switch off input voltage and current when thermocouple K2 attached onto R-circuit shows 50 ℃.
7. Wait for K2 to drop to 25 ℃.
8. Repeat this cycle three times from step 1 to determine the repeatability of the measurements.

Table 4. Data types obtained from sensors of vacuum chamber PWK1.

Reading	**Unit**
Voltage drop across MEDUSA	V
Current passed through MEDUSA	A
Tank pressure	hPa
Temperature of C-circuit (K1)	℃
Temperature of R-circuit (K2)	℃
Time	s

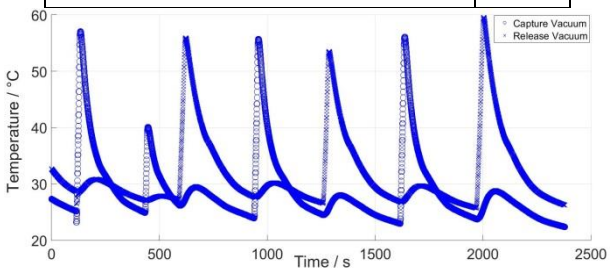

Figure. 8: C-circuit and R-circuit temperature data obtained during tests in a vacuum environment. These data were acquired while conducting four capture actions and three release actions in PWK1.

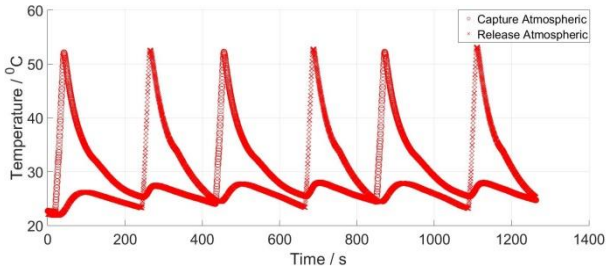

Figure. 9: C-circuit and R-circuit temperature data obtained during tests in an atmospheric environment. Data originated from conducting three capture actions and three release actions in PWK1.

Readings from thermocouple K1 and K2 may be subjected to a delay based on the physical connection deficiencies of the thermocouples. Also, differences in thermal connection between thermocouples K1 and K2 could cause an error in the data logged versus the actual

temperature of the arm.

Raw temperature data obtained from the vacuum tests are shown in Fig. 8 and Fig. 9. In the vacuum test four capture actions and three release actions were conducted. An extra capture action was conducted to test the thermocouple response. In the atmospheric tests, three capture actions and three release actions were conducted.

7 THERMAL DATA ANALYSIS

The data shown in Fig. 8 and fig. 9 were used to investigate the heating and cooling behaviour of the nitinol capture and release circuits for a range of input voltage and currents.

7.1 Temperature rise of C-circuit and R-circuit

The discussions on temperature data recorded during capture and release action is presented. The tests were conducted in both vacuum and atmospheric environments at room-temperature approximately between 21℃ to 24℃.

The data extracted includes the time taken to reach a specific temperature as it determines the time required to complete the capture and the release actions in both environments.

The electrical input was 9.89 V and 5.2 A to both C-circuit and R-circuit. The data sets given in Fig. 10 show the temperature changing with respect to time of the capturing nitinol wire (C-circuit) in both vacuum and atmospheric environment. The second data set in Fig. 11 shows the temperature changing with respect to time of the release nitinol wire (R-circuit). The two programmed shapes had different speeds of shape recovery was anticipated. The differently programmed shapes require specific amounts of electrical power to overcome the resisting forces from polyamide in the laboratory environment with the gravity vector aligned with the central axis of MEDUSA.

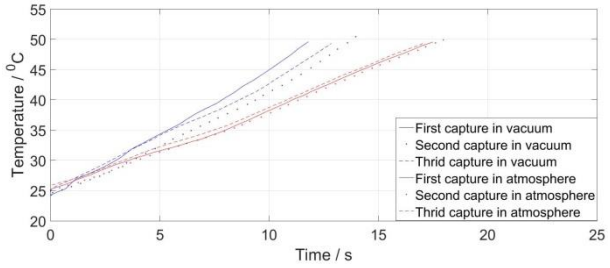

Figure. 10: Rising temperature of capture nitinol wire in vacuum and atmosphere. Three capture actions were conducted in both environments.

It is evident from both Fig.10 and Fig. 11 that the temperature rises faster in a vacuum compared to atmospheric environment. In a vacuum heat travels by two effects: conduction and radiation which causes heat to escape from nitinol at a slower rate in a vacuum than in atmosphere, where natural convection is present. Less time is required to reach the required temperature in a vacuum and hence less electrical power is required to operate MEDUSA in a vacuum environment.

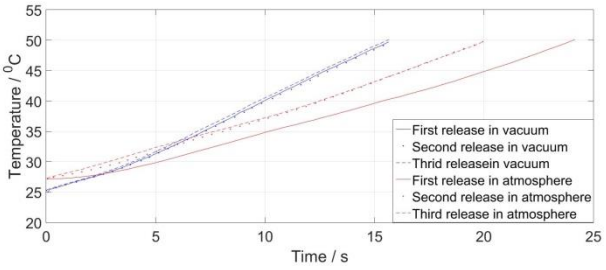

Figure. 11: Rising temperature of release nitinol in vacuum and atmosphere. Three release actions were conducted in both environments.

Furthermore, in both Fig. 10 and Fig. 11 a slight temperature gradient change was observed in the early stages of temperature rising. The dominating effect causing the temperature gradient change is the energy required during the state transition process due to the latent heat necessary for the transition. The energy consumption required for state transition was calculated using the latent heat from Tab. 1 which is 24200 J/kg and multiplying with volume and density of the wire leading to 178 J.

7.2 Temperature rise vs. input voltage and current

Two data sets were taken from the C-circuit data to compare the temperature rise in vacuum and atmosphere including the respective input voltage and current supplied (Fig. 12). It can be seen that the voltage and current was required for a shorter period of time in vacuum to reach the transition temperature. In a vacuum the C-circuit took 14 seconds of continuous current supply to reach 50 ℃ from 25 ℃ and in an atmospheric environment it took 18 s. The energy required to operate MEDUSA in vacuum was 700 J, compared to 900 J required to complete the same operation in atmosphere.

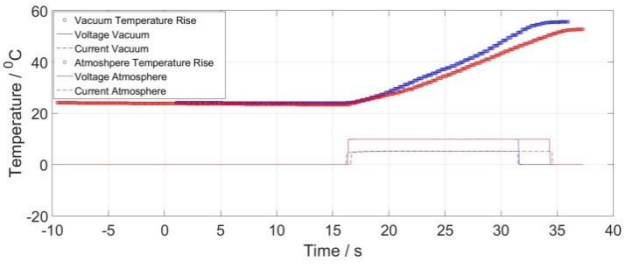

Figure. 12: Temperatures rise of capture nitinol in vacuum and atmosphere for an input voltage at 9.89 V and input current of 5.2 A.

7.3 Temperature decay measurements in vacuum and atmosphere

After actuation of the nitinol to complete a capture or release motion, the nitinol wires need time to cool down so that the wires no longer exert a force to return to their preprogramed state. This cooling down period defines the minimum delay between switching functionality from capture mode to release model.

According to test results in Fig. 13 and Fig. 14, the average time for the capture nitinol wire (C-circuit) to reach 25 ℃ from 50 ℃ in atmospheric conditions was approximately 200 s and 250 s in vacuum. The release nitinol wire (R-circuit) took 150 s in atmosphere and 300 s in vacuum. The prolonged temperature decay period in vacuum can be explained by the absence of convective cooling effects.

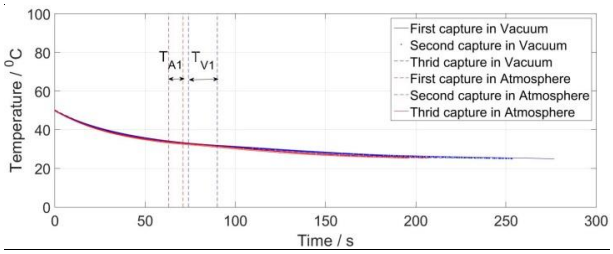

Figure. 13: Temperature decay during cool-down after closing of the capture arm in the vacuum and atmospheric environments.

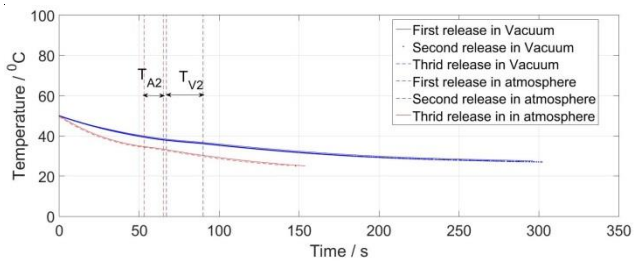

Figure. 14: Temperature decay during cool-down after opening of the release arm in the vacuum and atmospheric environments.

A possible explanation for the significant differences in temperature data between capture nitinol wire and release nitinol wire may be the difficult placing of the thermocouple on the thin nitinol wire which required large amounts of thermal conductive glue which may have led to conduction to other parts resulting in the data obtained. Further experiments will have to be done to understand the respective error.

One can clearly see another gradient change in both temperature data shown in Fig. 13 and Fig. 14. In Fig. 13 a change in gradient in the capture nitinol wire occurred in the time range marked as T_{A1} for atmosphere and T_{V1} for vacuum. In Fig. 14 a gradient change in the release nitinol wire occurred in the time range T_{A2} for atmosphere and T_{V2} for vacuum. This may be caused by the release of the latent heat as the nitinol transitioned from the Austenite state A_f back to the Martensite state M_s.

8 THERMAL ANALYSIS

In this section we discuss the thermal behaviour of MEDUSA observed in our experiments from first principle.

Heat travels by three effects in atmospheric environment: conduction, convection and radiation. Heat exchange via conduction with ambient particles will not occur in a vacuum due to the absence of particles needed for transmission. Given the non-conducting base of MEDUSA, radiation is the significant factor during heat exchange in vacuum.

8.1 Radiation heat flux density

According to the Stefan-Boltzman law, the radiation heat flux density equates the radiation energy dissipated on an area per second. The radiation heat flux density $\dot{q}$ in Equation 1 is directly proportional to both emissivity ϵ and Boltzmann constant σ and effective temperature to the power of 4 T^4. The emissivity of nitinol at 50 ℃ is ϵ = 0.66 [12].

A single capturing arm was the testing object used for this investigation. The heat flux lost due to radiation can be written as:

$$\dot{q}\mathrm{A} = \sigma\,\epsilon\,\mathrm{A}\,T^4 \qquad (1)$$

Where $\dot{q}$ stands for radiated heat flux density which is a function of T measured in Watt per square meters $[\frac{w}{m^2}]$ and A is the surface area of nitinol used where $A = 2\pi rl + 2\pi r^2$.

8.2 Heat balance equation of MEDUSA in vacuum

The input current supplied to the nitinol wires is a heat source during operation in vacuum, after a single command of capture or release action has completed, a cool-down time is required to allow heat exchange between nitinol and the ambient environment in order for the temperature to decay from 53 ℃ to 25 ℃. The total radiative heat flux from and to the nitinol is the sum of two expressions. The negative sign in Equation (2) denotes heat escaping from nitinol which is the simplified form of $\dot{q}$A from Equation (1) divided by V which is volume of nitinol wires used where $V = \pi r^2 l$.

$$\alpha(\mathrm{T}) = \frac{-2\,\epsilon\,\sigma\,T^4(r+l)}{rl} \qquad (2)$$

The primary heat source from ambient environment noted as β in Equation (3), where T_0 is the background temperature in Kelvin.

$$\beta = \frac{2\,\epsilon\,\sigma\,{T_0}^4(r+l)}{rl} \qquad (3)$$

The following term symbolizes the resultant temperature gradient change of the nitinol wires noted as γ:

$$\gamma = \rho\, C_p\, \frac{dT}{dt} \qquad (4)$$

Equating all three terms where α plus β equals to γ yields the resultant equation in Equation (5). The list of parameters used and their values are tabulated in Table 5.

$$\rho\, C_p\, \frac{dT}{dt} = \frac{-2\,\epsilon\,\sigma\,T^4(r+l)}{rl} + \frac{2\,\epsilon\,\sigma\,{T_0}^4(r+l)}{rl} \qquad (5)$$

Table 5. Parameters used in Equation 5.

Parameters	Definition	Value	Units
ρ	Density of nitinol	6500	$\frac{kg}{m^3}$
C_p	Specific heat of nitinol	320	$\frac{J}{kg.K}$
$\frac{dT}{dt}$	Temperature gradient	Function of time	$K.s^{-1}$
σ	Stefan-Boltzmann constant	5.670367×10^{-8}	$\frac{W}{m^2.K^4}$
ϵ	Emissivity	0.66	-
r	Radius of nitinol used	0.0005	m
l	Length of nitinol wire	1.44	m
T_0	Background temperature	293	K

Equation (5) was rearranged to $\frac{dT}{dt}$ and the resulting differential equation solved. Integrating both sides to get an equation as function of temperature with respect to time. Results are shown in Fig. 15 and compared to the data obtained in vacuum tests.

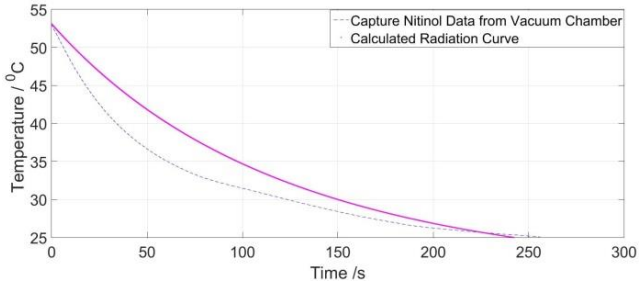

Figure. 15: Comparison of theoretical and observed temperature decay in vacuum. C-circuit data obtained from vacuum test was used to compare with values derived from Equation 5.

According to Fig. 15 the two functions started at the same temperature and took approximately the same duration to reach 25 ℃ from 53 ℃.

However, the two curves do not match especially in the region from $t = 20\,s$ to $t = 100\,s$. The deviation between the two may be because the theoretical curve derived from Equation 5 did not include the term of energy consumption during state transition from the Austenite state A_f to the Martensite state M_s. Secondly, Equation 5 did not include the factor that represents heat conduction between the hot nitinol wire and the polyamide body. The conduction between the nitinol wire and polyamide structure may explain the comparatively steep gradient in the beginning, as during this time the polyamide structure is still relatively cold leading to a good heat exchange. During the course of cool-down the polyamide structure warms up, as it receives heat from the wire and thus later delays the cooldown leading to a flattening of the gradient. In order to improve the accuracy of the graph derived from Equation 5, other significant heat exchange factors need to be included, including heat exchange between nitinol and the structure of MEDUSA.

9 CONCLUSION

The aim of this research was to investigate the potential application of shape memory alloys for space debris removal applications. The MEDUSA prototype was developed up to a Technology Readiness Level (TRL) of 4, which means that it had to be validated in a laboratory environment. The vacuum chamber (PWK1) in IRS provided a vacuum environment for testing. The prototype was also required to have a reversible operational ability to allow several capture attempts in a single space mission.

The capturing arms were designed to be rectangular and four 1 mm nitinol wires were chosen to provide the force needed to actuate the capturing mechanism. The material selected to manufacture the structure of the capturing arm was polyamide for its tolerating temperature, dampening ability and easiness to process. Protective covers for the arms were made out of Kapton HN which is suitable for this application. A method to construct the capturing arms was conceived and documented.

Fourteen capturing tests and thirteen release tests in total were conducted in the vacuum chamber PWK1 to compare the change in temperature gradient in both vacuum and atmospheric environments. The capturing process took less time to reach the transition temperature in vacuum which was with 14 s approximately 4 s quicker than in atmospheric environment. The shorter actuation time further results

in smaller total energy demand.

10 RECOMMENDATION

Based on our experiences from the work described above we propose a few recommendations were concluded for assembly and manufacturing inspections. The inspection would be an electrical inspection. This would ensure that the capturing function and the release function can be executed at command. The C-circuit and R-circuit should be tested with a very low current to demonstrate continuity with the capturing arms without raising its temperature appreciably.

11 REFERENCES

1. Feng, L.W.Y., Martinez, P., 2016. MEDUSA – Mechanism for Entrapment of Debris Using Shape memory Alloy. 67th International Astronautical Congress. Available at: https://iafastro.directory/iac/proceedings/IAC-16/ Accessed: 2017-01-02

2. Swartwout, M., 2013. The first one hundred cubesats: A statistical look.*Journal of Small Satellites*, *2*(2), pp.213-233

3. Kessler, D.J., Johnson, N.L., Liou, J.C. and Matney, M., 2010. The kessler syndrome: implications to future space operations. *Advances in the Astronautical Sciences*, *137*(8), p.2010.

4. Weeden, B., 2011. Overview of the legal and policy challenges of orbital debris removal. *Space Policy*, *27*(1), pp.38-43.

5. Johnson, N.L. and Stansbery, E.G., 2010. The new NASA orbital debris mitigation procedural requirements and standards. *Acta Astronautica*, *66*(3), pp.362-367.

6. National Research Council, 2011. *Limiting Future Collision Risk to Spacecraft: An assessment of NASA's Meteoroid and Orbital Debris Programs.* National Academies Press.

7. Liou, J.C., 2011. Active debris removal-a grand engineering challenge for the twenty-first century.

8. Wormnes, K., Le Letty, R., Summerer, L., Schonenborg, R., Dubois-Matra, O., Luraschi, E., Cropp, A., Krag, H. and Delaval, J., 2013, April. ESA technologies for space debris remediation. In *Proceedings of the 6th IAASS Conference: Safety is Not an Option* (pp. 3-4).

9. Novotny, M. and Kilpi, J., 2001. Shape memory alloys (SMA). Available at*: http://www. ac. tut. fi/aci/courses/ACI-51106/pdf/SMA/SMA-introduction. pdf*.

10. DiSalvo, F.J., 1999. Thermoelectric cooling and power generation. *Science*, *285*(5428), pp.703-706.

11. Herdrich, G., Fertig, M. and Löhle, S., 2009. Experimental simulation of high enthalpy planetary entries. *Open Plasma Physics Journal*, *2*, pp.150-164.

12. Song,.H, Kubica, E. and Gobet, R. Resistance modelling of sma wire actuators. In International workshop Smart Material Structure & NDT in Aerospace, page2.4.,2011